Egypt. J. Geo. **Vol. 66,** pp: 155-171 (2022)

Egyptian Journal of Geology
https://egjg.journals.ekb.eg

Structural and Stratigraphic Control on the Geothermal Regime of the Gulf of Suez, Egypt as Revealed by the Geophysical and Bottom-Hole Temperature Data

Hamed A. Alrefaee
Geology Department, University of Kafr Elsheikh, Egypt

BOTTOM-hole temperature measurements in the Suez Gulf, Egypt, were analyzed to assess the geothermal parameters of study area. The thermal gradient varies from 22 to 44°C/km, and heat flows from 45 to 118 mW/m^2. The highest thermal gradient and heat flow occur in Hammam Faraun-Ras Budran block and South Abu Zeneima at the eastern shoreline of the Gulf. High thermal gradient and heat flow also occur in Ras Gharib area at the Gulf western shoreline. Low thermal gradients and heat flow coincide with the basin of the Suez Gulf. The seismic sections were interpreted to reveal the impact of the local structural setting and stratigraphic succession on the geothermal parameters. The Bouguer anomaly map was analyzed to delineate the regional tectonic setting and its impact on the Suez Gulf geothermal regime. The magnetic data were used for calculating Curie depth point and examining any relationship or correlation with the geothermal parameters of the area. The geothermal reservoirs exist at South Abu Zeneima, Hammam Faraun, and Ras Gharib at the Suez Gulf coasts. It is possible to drill geothermal boreholes to obtain thermal water, which has a variety of uses.

Keywords: Geothermal regime, Gulf of Suez, Gravity, Magnetic, Seismic, Bottom-hole temperature data.

Introduction

Unlike conventional fossil fuels, geothermal energy is a renewable, safe, and clean natural form of energy that causes no pollution or global warming, making it a recommended energy source for industrial and domestic purposes. Geothermal energy emerged as an auspicious source of renewable energy to generate electricity in the face of the problem of the exhaustion of petroleum and gas reserves (Tester et al., 2007; Goldstein et al., 2011). Power plants utilizing geothermal energy do not require any fuel. Once a geothermal plant is constructed, no recurring money is needed for its operation. The Red Sea – Suez Gulf province is the most auspicious region for geothermal energy exploration. The province has a clustering of hot springs with considerable variations in temperature ranging from 3 to 72°C. The average geothermal gradient is 32°C/km in the whole area and exceeds 40°C/km in some localities. The heat flow ranges from 4 to 115 W/m^2 (Atef et al., 2016). The Egyptian territory, particularly the Suez Gulf, Aqaba Gulf, Red Sea, Sinai, and Eastern Desert, are promising geothermal provinces with abundant igneous rocks and hot springs (Swanberg et al. 1983). Moreover, these regions represent ideal localities for future investments in tourism and metallogeny sectors and hence represent attracting centers for laborers and workers.

Many researchers have studied the geothermal regime within the Suez Gulf area. The most significant studies are (e.g., Morgan et al., 1983; El-Qady et al., 2005; Lashin, 2013; Abdel Zaher et al., 2011; 2014). Earlier geothermal studies in Egypt utilized bottom-hole temperature and

*Corresponding author: hamed.elrefai@sci.kfs.edu.eg
Received: 28/11/2022; Accepted: 03/01/2023
DOI: 10.21608/EGJG.2023.177487.1031

geothermometers to assess the regional thermal gradients and heat flows. Recent geothermal studies involved geophysical techniques such as magnetic, gravity, resistivity, and magneto-telluric surveys besides the geothermal studies to outline the areal extension of possible geothermal reservoirs (El-Qady et al.2000, 2005; Abdel Zaher et al., 2012; Atef et al., 2016). The Suez Gulf represents a hopeful region for geothermal development where several hot springs exist, with the hot springs of Ayun Musa and Hammam Faraun having the highest temperatures (Swanberg et al., 1983). The typical geothermal gradient of the entire Gulf is about 27ºC/km, and the highest gradient is 48ºC/km in Hammam Faraun (Boulos, 1990). El-Fiky (2009) used geochemical techniques to reveal that Ras Sudr-2 well and Hammam Faraun have the hottest geothermal water, where the measured temperature of subsurface reservoir is 190.5ºC (Fig. 1). El-Qady et al. (2000, 2005) conducted resistivity surveys to outline a giant subsurface aquifer that is 100 m thick. They recommended drilling geothermal wells around the Hammam Faraun hot spring. Atya et al. (2010) utilized electromagnetic and vertical electrical sounding surveys to characterize the thermal reservoir at the Hammam Faraun and Abu Swiera.

Abdel Zaher et al. (2011) reported temperature gradients ranging between 24 and 45ºC/km and heat flows between 50 and 124 mW/m^2 around the vicinity of hot-spring on eastern shore of the Suez Gulf. Abdel Zaher et al. (2012) established a conceptual model for geothermal regime in the Hammam Faraun and stated that faults control the circulation of deep groundwater that feeds the hot spring. Lashin (2013) estimated moderately high thermal gradients that range from 22 to 30°C/km within the Suez Gulf and a superior high value (35-44 °C/km) for the Hammam Faraun area (Fig. 1). He also used geothermometers to conclude that Hammam Faraun spring has greatest formation temperature (95°C) at subsurface and highest flow of about 121.67 mW/m^2. Abdel Zaher et al. (2014) used bottom-hole temperature logs to calculate a thermal gradient ranging from 20 to 45 °C/km and a heat flow between 45 and 120 mW/m^2 at the eastern shore of the Suez Gulf. Atef et al. (2016) estimated an average gradient of 32°C/km in the Gulf with a local high value greater than 40 °C/km in some possible geothermal fields. They also estimated heat flow values between 45 and 115 mW/m^2. Abuzied et al. (2020) and Abdel Fattah et al. (2021) accomplished multidisciplinary studies on the Suez Gulf region to appraise new possible sites for geothermal energy.

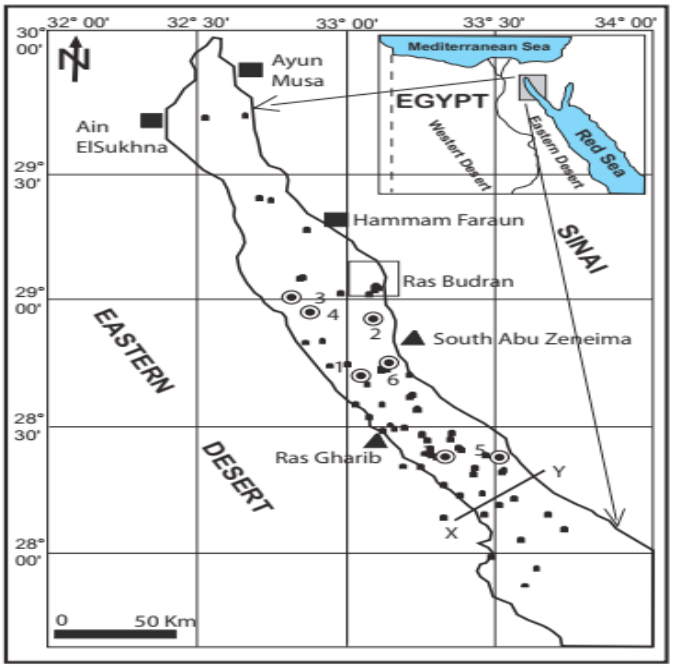

Fig. 1. The location map of Suez Gulf displays hot springs locations (big squares). Black square shows the Ras Budran 3D seismic survey. The two arrows show the boundaries of the area of gravity, magnetic, and geothermal data used in this study. The small squares show the wells' locations used to calculate thermal gradient and heat flow. Circles with numbers from 1 to 7 show the locations of wells used in true formation corrections. XY profile is the position of geological cross section (Fig. 3).

The current study utilizes borehole temperature data to evaluate geothermal parameters and explore possible geothermal reservoirs in the Suez Gulf area. Also, the study aims to investigate the possible influences of the structural and stratigraphic settings on the geothermal regime of the Suez Gulf area. The 3D seismic data will be used to image the subsurface structural and stratigraphic settings of the Ras Budran oil field to reveal possible influences of the structures and stratigraphic succession on the thermal parameters. In addition, gravity data will be employed to reveal regional tectonic setting and its influence on the geothermal regime of the Gulf area. Moreover, Curie depth point, estimated from magnetic data, will be checked to investigate its effect on the geothermal parameters.

Geology and tectonic setting

The Suez rift represents the northwestern extension of Red Sea rift that originated in the late Oligocene-early Miocene after departure of African and Arabian plates (Bosworth et al., 2005). During Late Miocene, activation of Aqaba transform fault decoupled the two rifts, and tectonic activity ceased in the Suez Gulf, whereas extension processes were active in Red Sea (Bosworth et al., 2012). The Gulf of Suez basin is an elongated trough with 300 km long and 60-80 km wide, separating the basement rocks of southern Sinai from those of Eastern Desert (Said, 1962). The Eocene and Cretaceous rocks, overlain by Miocene and younger rocks, form the coastal area. Moreover, elongated faulted blocks of the Precambrian basement and younger rocks border both sides of the coastal belt (Abdel-Gawad and Robson, 1970). The Gulf existed as an elongated embayment of the ancient Mediterranean Sea during the Carboniferous until the Late Cretaceous when the Alpine orogeny in the Pliocene closed the Tethys and resulted in the formation of the current Mediterranean Sea (Abdel-Gawad, 1969; Abdel-Gawad and Robson, 1970).

The rift of the Suez Gulf has a typical structural style of divergent margins. Main northwest-trending normal faults and minor northeast-trending faults dominate the rift (Thompson, 1976). The northwest-trending normal faults contribute to the complex structural array within the Gulf rift, including tilted blocks, asymmetric horsts, and half-grabens (Pivnik et al. 2003).

Harding (1984) categorized the sedimentary succession of the Suez Gulf into three cycles; pre-, syn-, and post-rift phases. Pre-rift stage comprises the Cambrian-Eocene rocks that rest on the basement rocks. These pre-rift rocks consist of a lower clastic section overlain by an upper carbonate unit. The lower clastic section consisted of the Nubia Sandstone and was deposited in continental and fluviomarine environments during the Cambrian to Lower Cretaceous. The upper section is known as Thebes Formation and is composed of marine carbonate, which was deposited during the Upper Cretaceous to Middle Eocene. In the Oligocene-Early Miocene, the Suez rift was associated with basaltic eruption, which resulted in northwest-trending dikes (Garfunkel and Bartov, 1977).

The syn-rift phase started after the rift establishment and with enough subsidence to be invaded by the sea during Early Miocene. Lower Miocene clastics dominated by shales and marls interbedded with Nukhul Limestone were deposited within a transgressive deep marine condition (Chowdhary and Taha, 1987). Tectonic uplift, faulting, and deep erosion followed the transgression process. By the Late Early Miocene, another transgression stage resulted in a relatively deep marine environment interrupted by short episodes of basin closing where lagoonal anhydrite of the Rudies Formation was deposited. The evaporites of the Kareem, Belaiym, and South Gharib Formations dominated the Middle Miocene, where they were deposited in a closed lagoon. The evaporites were interbedded with shale due to intervals of clastic influx. Sedimentation in a lagoonal basin dominated the Late Miocene, where the thick salt and anhydrite of the Zeit Formation were deposited (Chowdhary and Taha, 1987). Post-rift phase started in the Pliocene and was tectonically quiet. The post-rift sediments (post-Zeit) consist of coarse sandstone and conglomerates of the Pliocene and Pleistocene (Garfunkel and Bartov, 1977).

The Ras Budran oil field occupies an offshore region of the Suez Gulf approximately 4 km west of the Gulf's eastern shore (Fig. 1). Ras Budran occupies the southern corner of Hammam Faraun tilted block, which is situated within the central province of the Suez Gulf. Two main faults bound the Hammam Faraun block; Thal fault and Hammam Faraun coastal fault from the east and west, respectively (Fig. 2). The border faults extend northwest for approximately 25 km with a steep dip to the west (Moustafa and Abdeen, 1992). Hammam Faraun tilted block forms a half-graben structure

that dips to the southwest. Secondary structural features characterize the block, including faults, anticlines, and synclines that trend northwest and southeast. The pre-rift Paleozoic-Eocene rocks' sedimentary exposures and sparse syn-rift (Miocene) outcrops dominate the surface geology of Hammam Faraun tilted blocks (Moustafa and Abdeen, 1992). The stratigraphic succession of Hammam Faraun region consists mainly of sandstone, conglomerates, and limestones that belong to the Upper Cretaceous- post-Pliocene interval (Jackson et al., 2002).

Stratigraphic cross section of the investigated area (Fig. 3) has rock units that range from the Paleozoic to the Recent with several unconformity surfaces (Zahra and Nakhla, 2015).

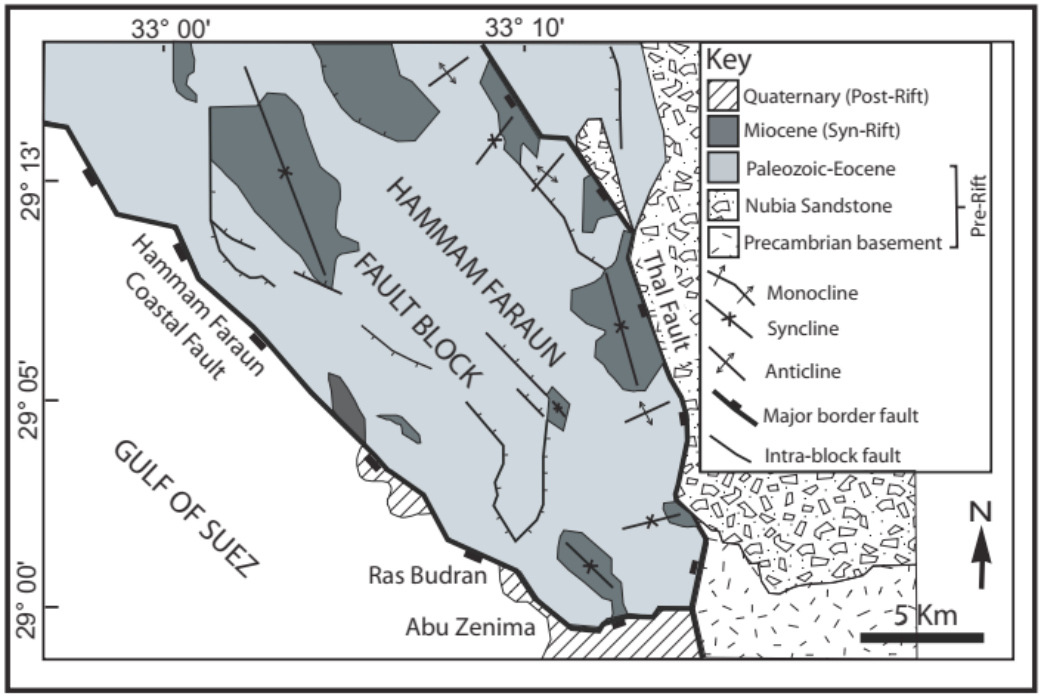

Fig. 2. Geologic map of Hammam Faraun faulted block (Moustafa and Abdeen, 1992).

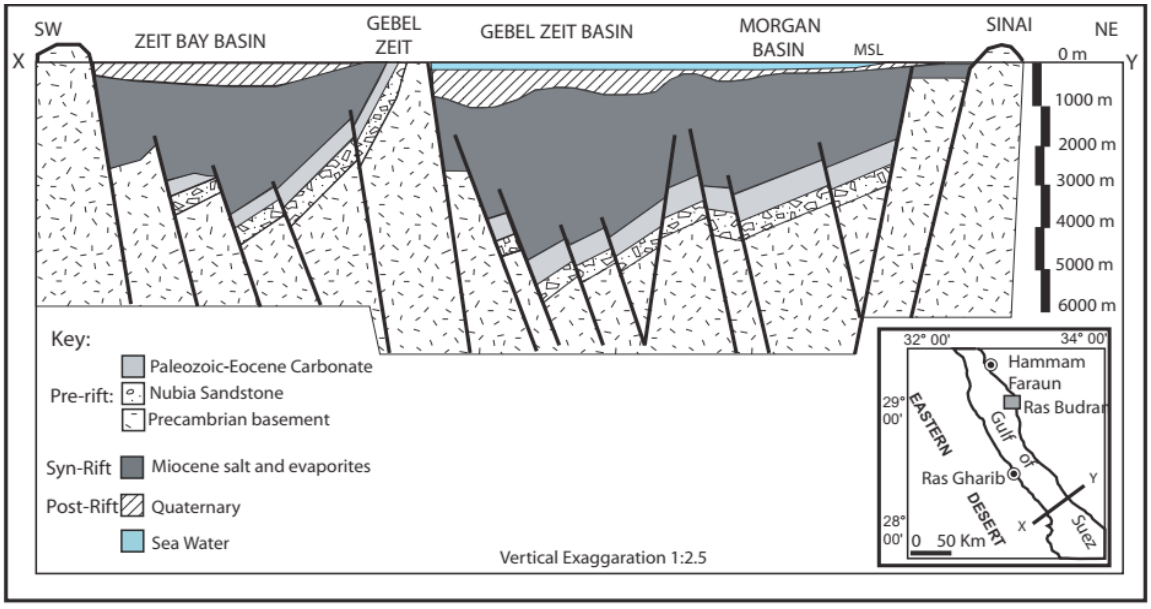

Fig. 3. The geologic cross section XY illustrating the stratigraphic succession and structural setting of Suez Gulf (United States Geological Survey, 1998).

Material and Methods

Geothermal data analysis

The most commonly used methods in geothermal exploration in Egypt are thermal gradient/heat flow estimates from deep drilled holes and geothermometer techniques (Morgan et al., 1983). In our current study, geophysical exploration of potential geothermal energy was performed using geothermal gradient/heat flow. The investigation began with the correction of bottom-hole temperature measurements recorded in oil boreholes in the Suez Gulf offshore to get the actual formation temperature.

Bottom-hole temperature correction

Temperature logs, either as continuous logs or as bottom-hole temperatures, are usually measured during drilling process or immediately after the circulation of drilling fluid stops. During the period between the cessation of drilling fluid flow and acquiring temperature measurements, there is usually a loss in the formation temperature (Lashin, 2013). The cold drilling fluid results in a cooling effect by invading the warmer formation lithology through a convection process (Atef et al., 2016). The drilling fluid reduces its temperature below the actual formation temperature (Peters and Nelson, 2009). Correcting formation temperatures are needed to calculate the heat flow and geothermal gradient. Bottom-hole temperature records are corrected to actual formation temperature using corrections by Horner (1951) and Waples et al. (2004) (Table 1).

The correction process using Horner (1951) and Waples et al. (2004) shows that the adjusted actual formation temperature by the two methods is close to each other. The difference in most cases is about ± 7 - 9 degrees. These two corrections are described in the following two paragraphs. Successfully using Horner's correction method requires at least three logging runs of temperature and time for each run (Fig. 4). Horner's correction also needs accurate records of the times since drilling fluid circulation stopped and the duration of circulation time (Peters and Nelson, 2009). Horner's correction method involves plotting bottom-hole temperature on a linear vertical scale against T/(T+t) on a logarithmic horizontal scale. Where (T) is time since drilling fluid circulation ceased and (t) is duration of circulation time needed for formation cooling (Horner, 1951). Accurate corrected formation temperature is found by extrapolating a least squares regression line that best fits the three data points (Fig. 4).

Because reliable Horner's correction requires at least three logging runs, which is not the case for most of the available data, Waples's correction was used to correct the entire temperature dataset. Waples's method depends on the accurate time estimation since drilling fluid circulation stop (TSC) and depth. Corrected actual formation temperature is obtained using the formula:

$$T\ true=Tsurface*(T\ measured-T\ surface)\ -0.001391\ (D-4498) \quad (1)$$

where the $T_{measured}$ refers to the measured log temperature in Celsius, (D) refers to depth beneath sea bottom in meters, and $T_{surface}$ represents the temperature measured at ground surface. Correction factor (F_S) is dependent on the ($T_{SC)}$ and calculated as:

$$Fs=(-0.1462*\ -ln\ ---(Tsc)+1.699)/\ (0.527*Z\text{^}0.075)- \quad (2)$$

TABLE 1. Correction of bottom-hole temperature for selected wells using Horner's (1951) and Waples et al. (2004) methods.

No.	Well Name	Bottom hole temperature °C	Horner's Correction	Waples's Correction
1	ARM-1	108.89	120	129
2	BEL 113 M-11	93.33	110	112.33
3	GG-83-3	84.44	98	95.96
4	HH83-1	71.11	73	80.89
5	MM-86-1A	127.22	143	152
6	SB268-1/1A	122.78	132	125.75
7	Shukeir Bay	72.22	83	91.2

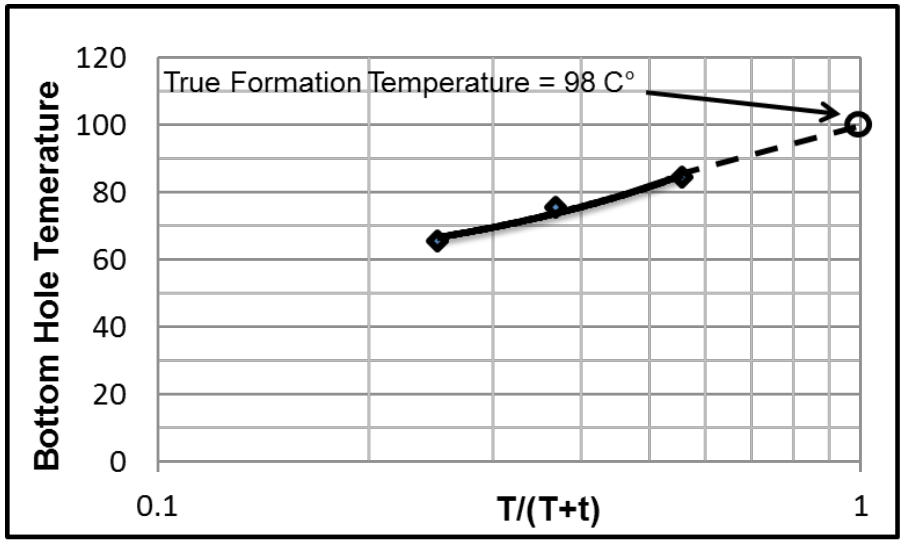

Fig. 4. Horner's correction for the well GG83-3 shows the plot of the bottom-hole temperature on a linear vertical scale against T/(T+t) at a logarithmic horizontal scale. T refers to time since circulation stopped, and t represents circulation period. The extension of the least square regression line that best fits the three data points intersects the vertical line with the value one on the T/(T+t) axis in a point, which represents the true formation temperature.

Geothermal parameters calculations

The geothermal gradient for (70) offshore oil wells was calculated for each well, assuming the temperature at the sea bottom to be 26.7°C (mean annual surface temperature in Egypt assumed by Morgan et al. (1983). The geothermal gradient (G.G) was calculated as follows:

$$G.G=\Delta T/\Delta Z=((T2-T1)/(Z2-Z1))*1000 \quad (3)$$

Where (ΔT) refers to temperature variation in the (Z2–Z1) depth interval measured in meters.

The map of geothermal gradient shows values that range from 22 to 44°C/km (Fig. 5a). The highest thermal gradient (shown as magenta color) occurs in several zones, including the Hammam Faraun-Ras Budran block (T1) and Abu Zeneima (T2) at the Gulf eastern coast. Also, high thermal gradients exist at Ras Gharib (T3) on the Gulf's western coast and the entrance of the Suez Gulf (T4). The thermal gradient decreases at the central and northern parts, where lowest values (blue color) coincide with the troughs of the Gulf basin.

Heat flow (H) was estimated using the formula $H=C^*(\Delta T/\Delta Z)$, where (C) refers to the geothermal conductivity, and $(\Delta T/\Delta Z)$ refers to a temperature gradient. Table (2) demonstrates the geothermal conductivities of the different subsurface rocks in studied area. Heat flow varies between 46 and 118 mW/m^2 (Fig. 5b) and follows the same configuration as the thermal gradient. The map shows high heat flow values (magenta color) in Hammam Faraun-Ras Budran block (T1) and Abu Zeneima (T2) along the eastern coast of the Gulf and Ras Gharib (T3) along the western coast. Like the gradient, heat flow decreases at the central and northern parts, where low heat flow (light blue color) coincides with the basin of the Gulf.

Seismic data analysis

The seismic survey of the Ras Budran field covers mainly an offshore area. It extends to the east to include a coastal area (Fig. 1). The seismic survey has a total surface area of 50 km^2 with a production area of 15 km^2. The 3D seismic data were obtained by merging two 3D seismic surveys acquired by Western Geophysical Company (El-Hateel, 2013). The first is a marine seismic survey acquired by a streamer in 1980 and covers the northwestern, western, and central regions of the Ras Budran oil field. The second was acquired by ocean bottom cables in 1997 and covered the eastern part of the survey. The final merged seismic survey was subject to conventional 3D seismic processing. The processed seismic data are represented by post-stack depth migration (Fig. 6). Four wells with formation tops were utilized to identify the seismic reflector (stratigraphic horizons) to facilitate the interpretation process (Fig. 6).

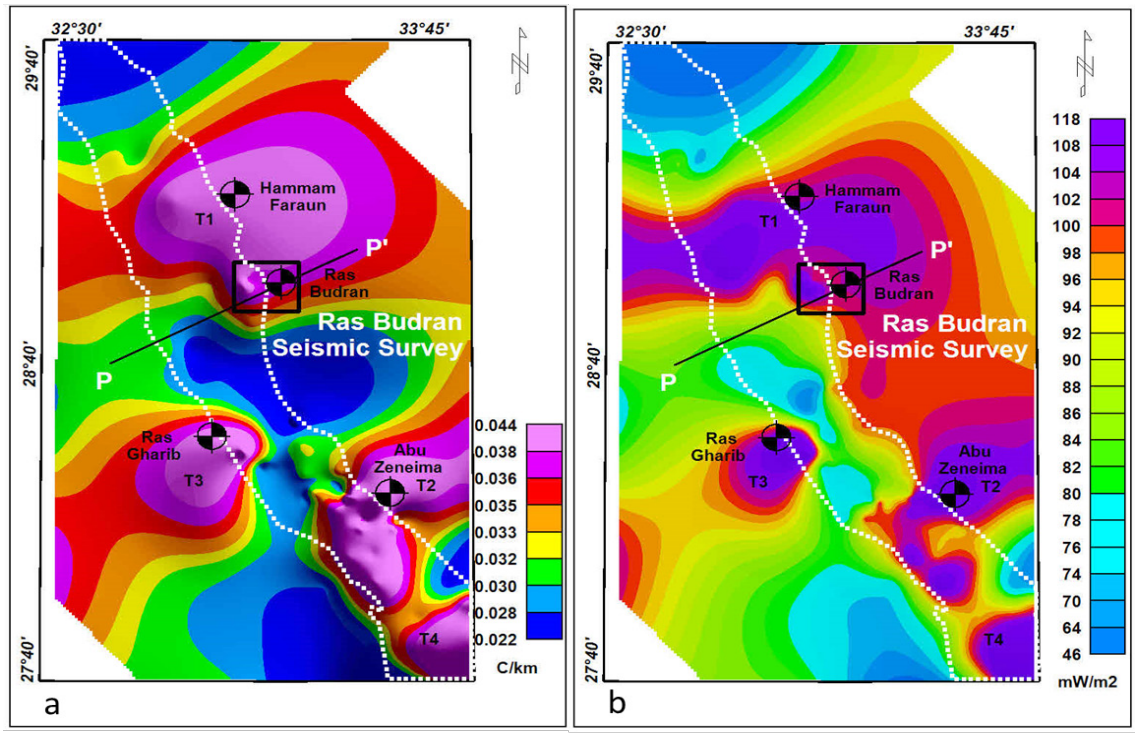

Fig. 5. a. Geothermal gradient varies from 22 to 44 C/km with the highest values at the eastern margin (T1 at Hammam Faraun and T2 at Abu Zeneima) and western margin (T3 at Ras Gharib). The low gradient coincides with the Gulf basin. b. Heat flow varies from 46 to 118 mW/m2 and follows the same pattern as the thermal gradient.

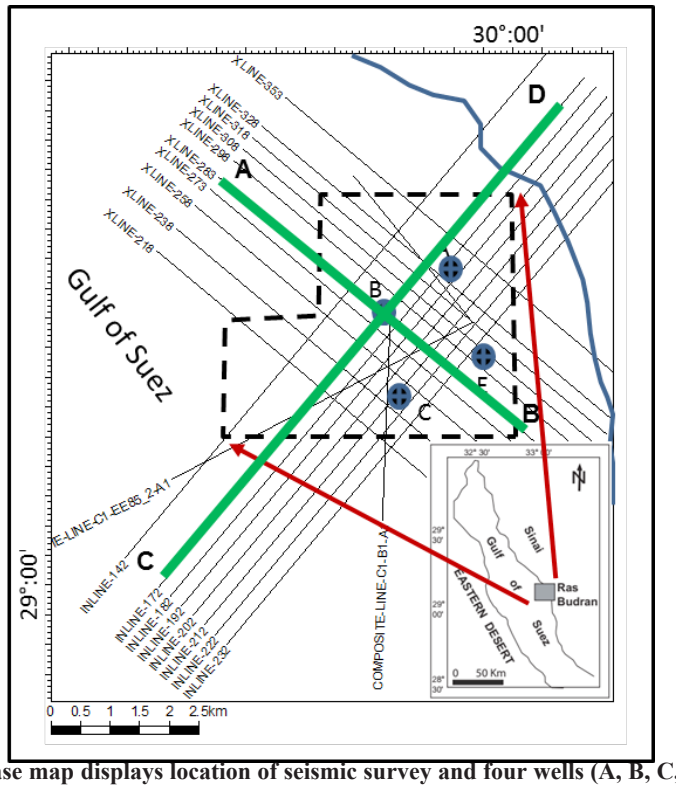

Fig. 6. The Ras Budran base map displays location of seismic survey and four wells (A, B, C, and E). AB and CD are the locations of seismic profiles displayed in figures 7 and 8, respectively.

TABLE 2. Thermal conductivities of different lithological units measured from drill cutting samples from boreholes within the Suez Gulf (Morgan et al., 1983; Boulos, 1990).

Lithology		Conductivity (W/m/K)
Pre-rift sediments	Precambrian Basement	3.1
	Cambrian - L. Cretaceous Nubia Sandstone	2.7
	Cretaceous – M. Eocene Carbonate	2.4
Syn-rift sediments	Miocene Shale, Evaporite, Salt	2.3
Post-rift sediments	Sandstone and conglomerates	2.2

The seismic profile (AB) illustrates the structural elements of the Ras Budran oil field (Fig. 7). The upper section consists of the undeformed post-rift (post-Zeit) formations underlain by syn-rift sediments of the Miocene. The Miocene syn-rift succession consists of an upper section, which includes Kareem, Belaiym, Zeit, and South Gharib formations (Middle to Upper Miocene), and a lower section, which includes Nukhul and Rudie's formations (Lower Miocene). Lower section of syn-rift sequence is deformed by faulted blocks, forming grabens and horsts. Normal step faults with great throws dominate the pre-rift sequence (Eocene Thebes carbonate rocks, the Paleozoic-Cretaceous Nubia Sand, and the basement). The faults strike northeast-southwest direction perpendicular to axis of the Gulf.

The seismic profile (CD) illustrates that a dragging fold deforms the upper syn-rift section. In contrast, the lower syn-rift section is deformed through normal faults having opposite dips, resulting in grabens and horsts (Fig. 8). Normal step faults deform the pre-rift section. Also, a major fault with a large vertical throw cuts through the entire section. The fault uplifts the pre-rift (basement rocks, Nubia Sandstone, and Eocene) and syn-rift sections at the right-hand side. The faults strike NW-SE direction similar to the Gulf axis.

Gravity and magnetic data analysis

Bouguer gravity map shows a northwest-trending elongated gravity low (NG1). The low gravity corresponds to the Gulf basin and varies from 35 to 80 mGal (Fig. 9.a). The gravity low is bounded by prominent gravity highs (PG1 and PG3) to the east, related to the uplifted basement exposures bordering the eastern shore of the Suez rift and exposures of Sinai Massive igneous rocks. Also, a linear moderate gravity anomaly (PG2) and high gravity (PG4) border the Gulf from the west. The RTP map shows a low magnetic anomaly (NM1) that coincides with Gulf basin (Fig. 9.b). The map also shows high magnetic anomalies (PM1 and PM2) at the Gulf's central and southern entrance, respectively.

The tilt derivative of the horizontal derivative (TDX) is also known as the normalized horizontal derivative (NHD) and is defined as the ratio between horizontal gradient and vertical derivative. TDX displays a maximum gravity overhead the dense body edges and distinguishes edges better than tilt angle. The TDH is calculated using the formula of Cooper and Cowan (2006):

$$TDX=atan\ \sqrt{((dG/dx)^2+(dG/dy)^2)}/((dG/dz)) \quad (4)$$

Where $\sqrt{((dG/dx)^2+(dG/dy)^2)}$ is the horizontal gradient, and dG/dZ is first vertical derivative.

Theta map determines edges with high accuracy Wijns et al. (2005), and can be computed by the equation:

$$Theta\ or\ Cos\ \Theta = HG/TG \quad (5)$$

Where HG denotes the horizontal gradient, and TG denotes the total gradient.

Tilt angle of the horizontal gradient (also known as TAHG) produces gravity maxima above the source edges and responds equally to the deep and shallow sources. The TAHG shows edge location more accurately than the several edge detection methods, even in the presence of numerous interfering bodies. TAHG is estimated through the formula by Ferreira et al. (2013):

$$TAHG=atan\ (\partial THDR/dz)/\sqrt{((\partial THDR/dx)^2+(\partial THDR/dy)^2)} \quad (6)$$

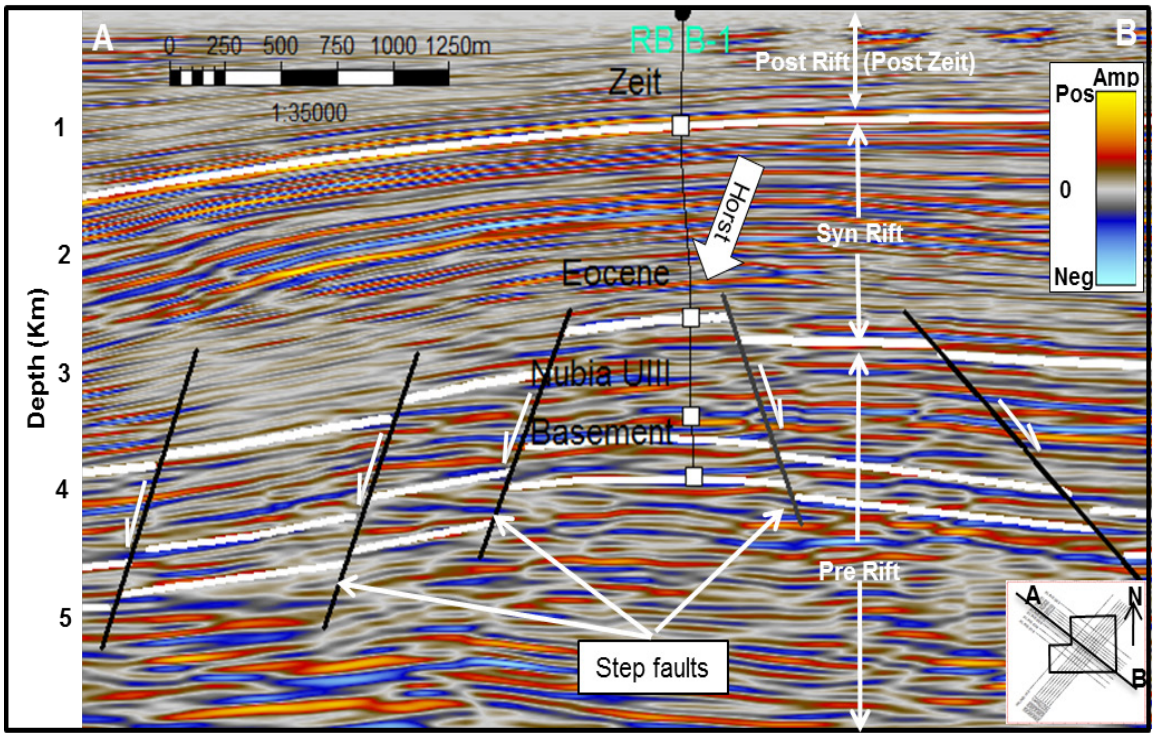

Fig. 7. Vertical seismic section (AB) illustrating the subsurface structures of the Ras Budran. Lower Miocene is deformed by faulted blocks, forming horsts and half-grabens. Normal step faults deform the pre-rift section.

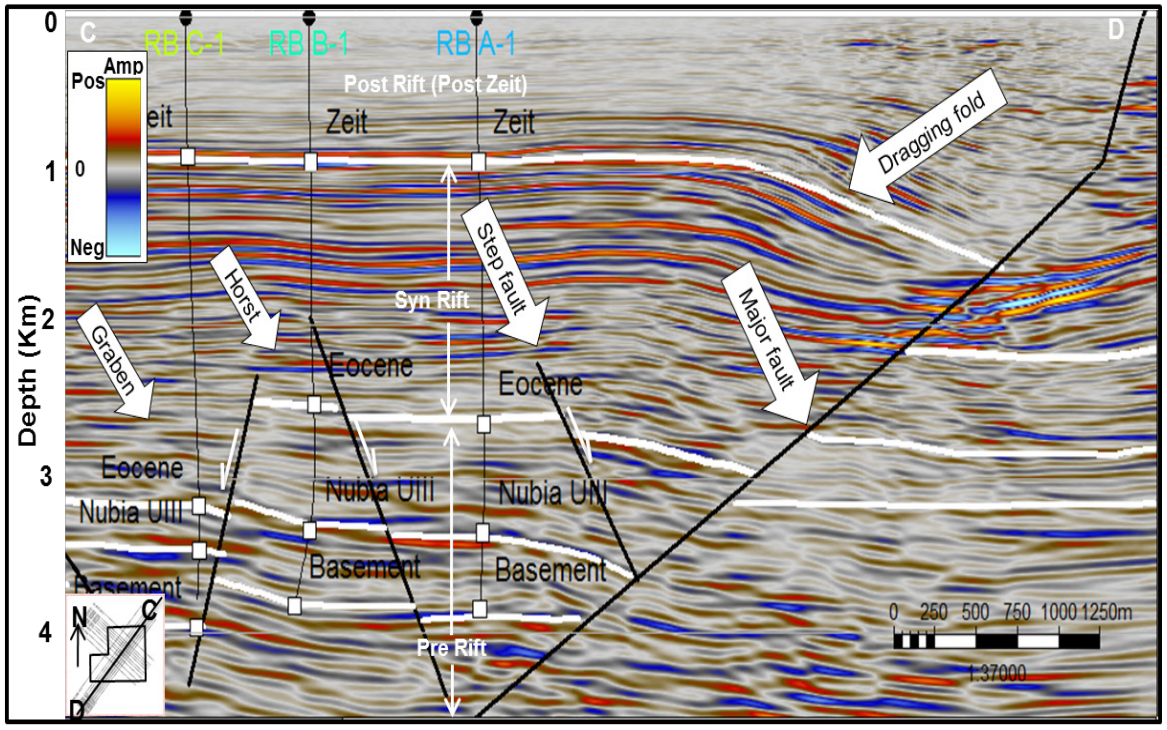

Fig. 8. Vertical seismic profile CD shows a dragging anticlinal fold deforming the upper section of Miocene syn-rift rocks, whereas horsts and grabens deform lower section. Normal step faults deform the pre-rift section. A major fault extends from the basement to the surface.

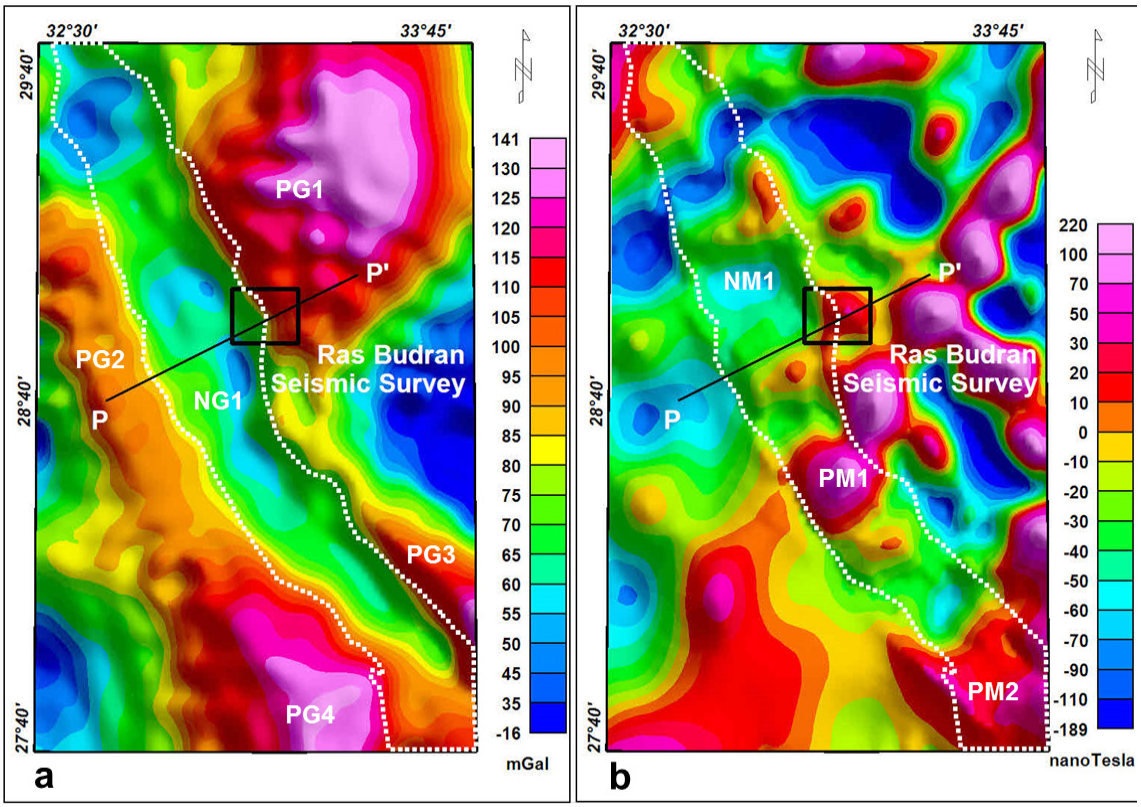

Fig. 9.a. The Bouguer anomaly map shows Ras Budran's seismic survey location (black square). NG1 points to low gravity coinciding with Gulf basin, and (PG1, PG2, PG3, and PG4) refer to positive gravity anomalies described in the text. b. The RTP map shows low magnetic anomaly (NM1) coinciding with Gulf basin. PM1 refers to high magnetic anomaly at the central portion of the Suez Gulf, and PM2 is a high magnetic anomaly at the Gulf.

In the current study, TDX, TAHG, and Theta map (θ) of the Bouguer data shows two northwest-trending linear gravity maxima on the two margins of the Suez Gulf (Fig. 10). The two gravity maxima have regional extensions and are parallel to each other. These three maps/two maps show gravity maxima above edges of the dense bodies or the faults. These two gravity maxima may indicate two regional rift faults that outline the margins of the Gulf.

A 2D gravity model that extends NE-SW along the profile (PP´) and passes by the Ras Budran seismic survey was built for imaging subsurface structural setting (Fig. 11). The interpreted surfaces and faults from seismic data were used to constrain the model. The densities of rock units were obtained from previous studies (Azab and El-Khadargy, 2013; Ahmed et al., 2014; Araffa et al., 2020). The subsurface rock units beneath the Gulf area were assigned various densities. The basement rocks were assigned a density of 2.67 gm/cc, pre-rift rocks 2.5 gm/cc, syn-rift rocks 2.3 gm/cc, post-rift rocks 2.2 gm/cc, and the seawater 1.03 gm/cc. The right-hand side of the model shows gravity high (PG1) that corresponds to the exposed basement rock of southern Sinai Complex and the uplifted basement rocks of the eastern rift shoulder. A gravity low (NG1) follows the gravity high in the western direction and coincides with the Gulf basin. The left-hand side shows a moderate to gravity high (PG2) value corresponding to the uplifted basement blocks of the rift's western shoulder.

Curie point depth calculation

Calculating Curie depth point (CDP) represents a complex task since the magnetic signals from the upper surfaces of the magnetized bodies dominate signals from the bottom surfaces at the whole wavelength ranges (Blakely, 1995). The depth to lower surface of a magnetized source is estimated from power spectrum curve (Fig. 12a and b).

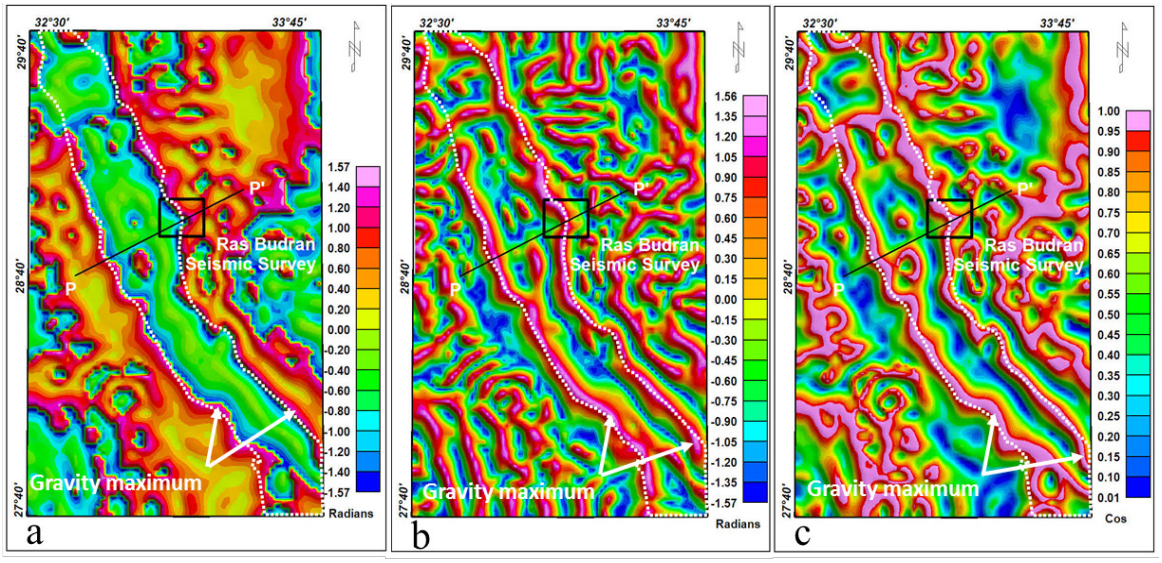

Fig. 10.a. Tilt derivative of horizontal derivative (TDX), b. tilt angle of horizontal gradient (TAHG), and c. Theta map of gravity data showing gravity maxima the Gulf coasts. The maps also show locations of Ras Budran seismic survey (black square) and the 2D gravity profile PP'.

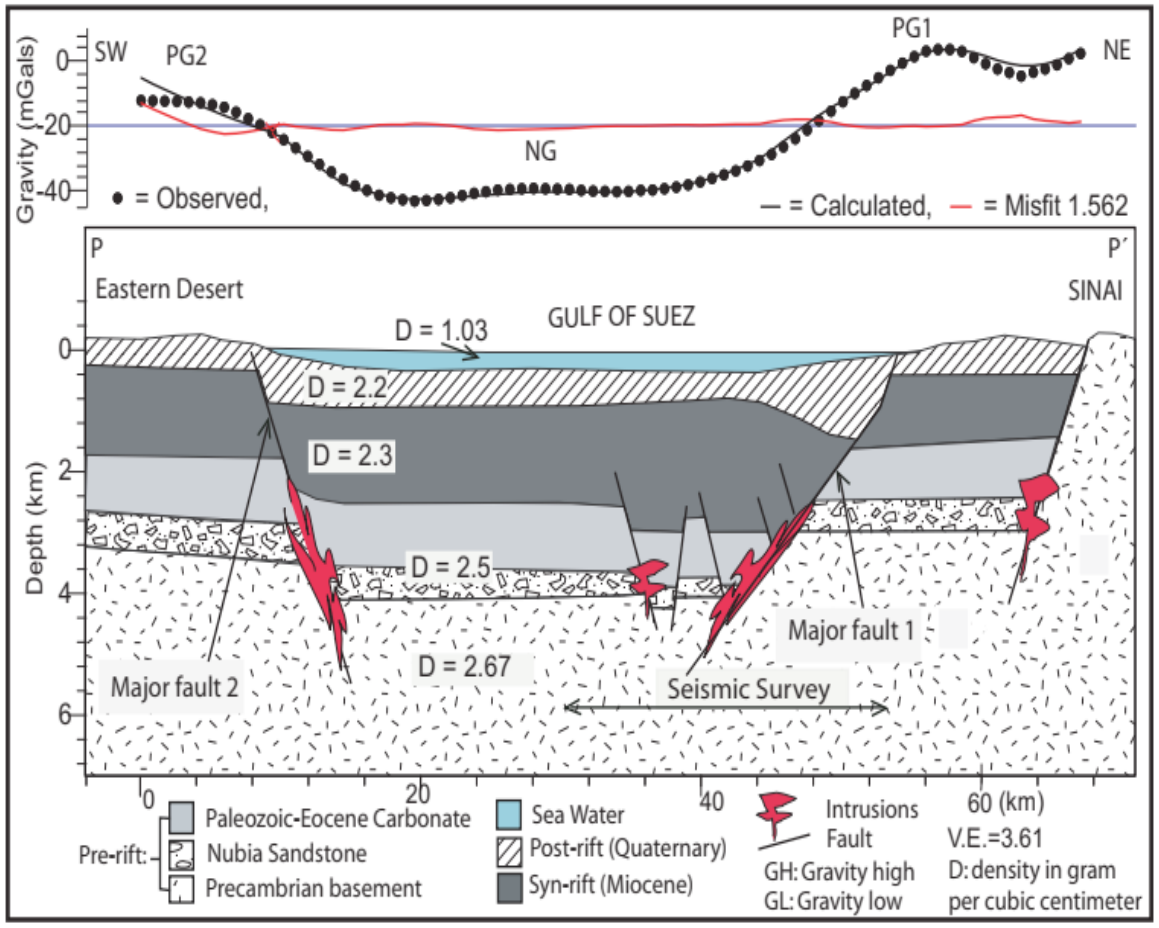

Fig. 11. A 2D gravity model extending along the profile PP shows subsurface geology below the Suez Gulf.

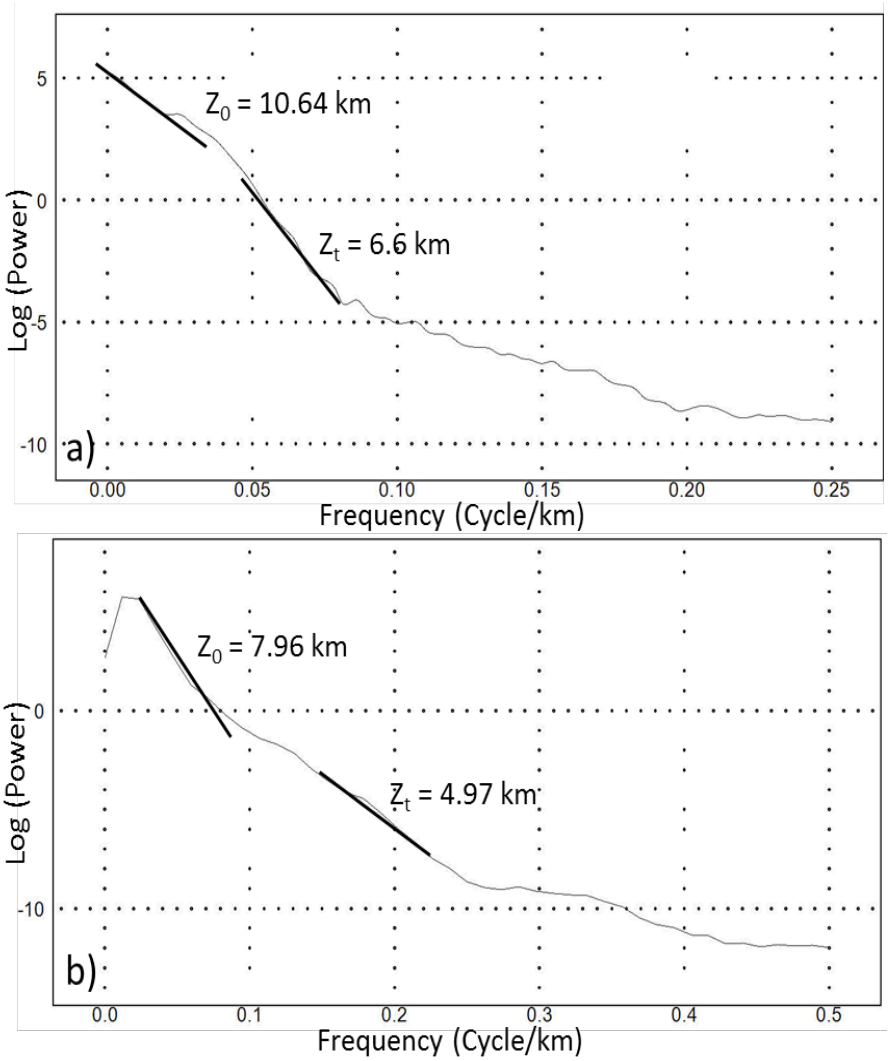

Fig. 12. a. The magnetic power spectrum of the entire area. b. power spectrum of subregion (1). The linear fitting estimates the depths to the top of the magnetized body (Zt) and centroid (Z0).

In the current study, the CDP was calculated using the technique of Tanaka et al. (1999). The technique provides a two-procedure technique that utilizes the spectrum analysis (Spector and Grant, 1970) for determining bottom depth (Zb) of the deepest magnetic bodies. The centroid depth of the magnetized source (Z0) and depth to the upper surface (Zt) are estimated in such a technique. The Z0 and Zt are estimated via fitting the line segment through low and high wavenumber portions of power spectrum of the ln [ΦΔT(|k|)1/2] and {[ΦΔT(|k|)1/2]/ |k|}. The magnetic power spectrum is denoted by (ΦΔT) and wavenumber by k. Consequently, the Curie depth point (Db) is computed using the following formula:

$$Db = 2D0 - Dt \quad (7)$$

The Curie depth point map illustrates that the Curie depth has its maximum value of 10600m in the northeastern area and decreases to 8600m at Hammam Faraun and 7400 m at Ras Budran. The Curie depth decreases as moving northwest to 5000m and southward to 6500m at Ras Gharib, then 5400m at Abu Zeneima (Fig. 13). There is an inverse relationship between the Curie depth point values and the geothermal parameters with an exception (Fig. 5 a and b). In the southern regions, the shallow Curie depth point values at Abu Zeneima, Ras Gharib, and the southern entrance of the Gulf coincide with high gradient and heat flow values. The northern regions exhibit moderately deep Curie depth in Hammam Faraun and Ras Budran match with high gradient and heat flow.

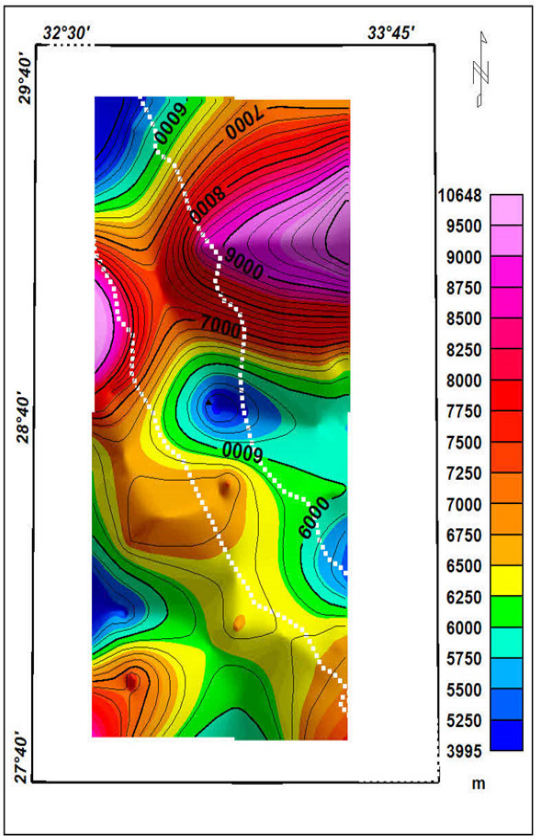

Fig. 13. Curie depth point map of Suez Gulf area.

Results and Discussion

The highest thermal gradients (38-44 C°/km) and heat flows (104-118 mW/m^2) occur at four distinct zones; the Hammam Faraun-Ras Budran block, South Abu Zeneima at eastern shoreline of the Gulf, Ras Gharib at the western shoreline, and southern entrance of the Gulf (Fig. 5 a and b). The high thermal gradient and heat flow at these localities are related to major rift faults that define the Gulf margins. Presence of the major rift faults is indicated by the seismic section (CD) (Fig. 8) and gravity section (Fig. 11). The major rift fault (the biggest fault shown on the right side) extends in the northwest-southeast direction parallel to Gulf at the eastern edge of the Suez Gulf. The major fault extends from the deep basement rocks through the Nubia Sandstone to the sea bottom. Additional evidence of the presence of the major rift faults comes from the gravity maxima shown by the edge detection maps, which display gravity maxima coinciding with the Gulf margins (Fig. 10). Moreover, 2D gravity model shows high gravity anomalies (PG1 and PG2) above western and eastern shorelines of the Suez Gulf (Fig. 11). The high gravity anomalies match with the upthrows of the major rift faults, whereas the low gravity anomalies match with downthrows. On the one hand, the upthrows of the major rift faults brought the Precambrian basement blocks with high densities to shallower depths at the margins of the Gulf. As a result, the high gravity anomalies (PG1, PG2, PG3, and PG4) are related to uplifted basement block of the rift shoulders on Gulf coasts. On the other hand, at downthrows of major rift faults, the Precambrian basement blocks exist at greater depth and are overlain by a thick sedimentary cover with low densities. Consequently, the low gravity anomaly (NG1) coincides with the downthrown basement block of the Gulf basin (Figs. 9a and 11). These observations agree with previous results of Abdel Zaher et al. (2012) and Atef et al. (2016), who related high gravity to the rift faults. In addition, the geothermal parameters seem to be affected by the Curie depth point. Thermal gradient and heat flow have high values at the localities of the shallow Curie depth point, whereas the localities with deep Curie depth points have low geothermal gradients and heat flow.

Low heat flows and thermal gradients in the Gulf are interrelated to low thermal conductivities of syn-rift sediments (Miocene salt and evaporites) and post-rift sediments (Table 2). The syn- and post-rift sediments have thick sedimentary successions, as indicated by Figures (3 and 11). This conclusion agrees well with the results of Tewfik et al. (1992), who reported a clear correlation between the geothermal trends and the pre-Miocene relief (pre-rift relief) in the Gulf. The high geothermal trends accompany shallower (uplifted) pre-rift blocks, whereas low trends are associated with downthrown (deeper) pre-rift blocks. Therefore, high gradients and heat flows are due to the Gulf rift faults that agree with previous results by Issar et al. (1971) and Morgan et al. (1983). The geological cross section (Fig. 3) and the 2D gravity model (Fig. 11) show that the uplifted pre-rift rocks (basement and Nubia Sandstone) that have high thermal conductivities values are overlain by thin sections of syn- and post-rift sediments. The seismic section (CD) reflect that the trough of the Gulf basin is filled with a thick sedimentary section of the syn-rift, whereas the margin of the Gulf is filled with a thin section (Fig. 7). The syn-rift sediments have low thermal conductivities, which contribute to the low thermal parameters in the trough of the Gulf basin. The low geothermal parameters are associated with the downthrown basement and Nubia Sandstone rocks overlain by a thick cover of syn-rift (salt and evaporites) and post-rift sediments that fill the Gulf basin, which agree with the conclusions by Tewfik et al. (1992). Low thermal gradient and heat flow (Figs. 5) in the Gulf center show a clear correlation with the low gravity (NG1) of the trough of the Gulf basin (Fig. 9a). The low gravity (NG1) is due to thick sedimentary cover (syn- and post-rift) that fills the Gulf depocenter as indicated by the 2D gravity model (Fig. 11). Since Hammam Faraun spring and Ras Budran oil field are close to each other and belong to the same fault block as shown in Figure (2), by analogy, their stratigraphic and structural settings are mostly the same. In the Ras Budran, the seismic data show that the Nubia Sandstone (geothermal reservoir) is highly deformed by faults that extend upwards to the Eocene, and younger formations then reach the sea bottom. Issar et al. (1971), Morgan et al. (1983), and El-Fiky (2009) stated that the Nubia Sandstone is a promising geothermal reservoir in the Suez Gulf province. From seismic data, Nubia Sandstone occurs at depths ranging from 4000 to 6000m. So, geothermal wells can be drilled, and power plant stations constructed to produce hot thermal water, which can be used for several purposes, such as domestic purposes, fish farming, swimming pools, and treatment.

Conclusions

The current study represents a multi-disciplinary approach, which devote several datasets including gravity, magnetic, bottom-hole temperature, and seismic data. The current research is an integrated pioneer study to reveal the effects of the stratigraphy and structural elements on the geothermal setting in the Suez Gulf area. The stratigraphy and structural setting mainly control the geothermal regime of the Suez Gulf. High geothermal gradient and heat flow coincide with the major rift faults, which define the Gulf margins, whereas the low values coincide with the trough of the Gulf basin. The uplifted (shallower) basement and pre-rift rocks with high thermal conductivity contribute to the high thermal parameters at the gulf coasts. The thick syn- and post-rift sediments with low thermal conductivities contribute to the low thermal parameters in the Gulf basin. The distribution of the geothermal parameters' values shows a clear, direct correlation with the gravity anomalies and a reverse correlation with the Curie point depth. Low-temperature geothermal reservoirs could exist in the subsurface of the Hammam Faraun, South Zeneima, and Ras Gharib, which have the highest thermal gradient (44°C/km) and heat flow (118 mW/m^2). Binary power plants can be constructed where deep geothermal wells are drilled to reach the Nubia Sandstone geothermal reservoirs. The power plants can generate low-voltage electricity or injects thermal water or vapor, which can be used in many utilities such as worming, fish farming, and swimming pools.

Acknowledgment

The author is grateful to the EGPC for providing temperature measurements from boreholes in the Suez Gulf region. I wish to thank the Suez Oil Company (SUCO) for providing the 3D seismic and well logging data for Ras Budran Oilfield, Offshore Gulf of Suez. I also want to acknowledge the Bureau Gravimétrique International (BGI) for providing Satellite Gravity data.

References

Abdel-Fattah, M.I., Shendi, E.A.H., Kaiser, M.F. and Abuzied, S.M., (2021) Unveiling geothermal potential sites along Gulf of Suez (Egypt) using an integrated geoscience approach. *J. of Terra Nova*, **33(3)**, 306-319.

Abdel-Gawad, M., (1969) New evidence for transcurrent movement in the Red Sea and petroleum implication. *Amer. Assoc. of Petr. Geol. Bull.*, **53**, 1466-1479.

Abdel-Gawad, M., Robson, D.A., (1970) The Gulf of Suez: a brief review of stratigraphy and structure. *Philosophical Transactions of the Royal Society*, **A 267**, 41–48.doi:10.1098/rsta. 1970.0022

Abdel Zaher, M., Saibi, H., El Nouby, M., Ghamry, E., Ehara, S., (2011) A preliminary regional geothermal assessment of the Gulf of Suez, Egypt. *J. Afr. Earth. Sci.*, **60**, 117–132.

Abdel Zaher, M., Nishijima, J., El-Qady, G., Aboud, E., Masoud, O., Soliman, M., and Ehara, S., (2011) Gravity and Magnetotelluric Investigations to Elicit the Origin of Hammam Faraun Hot Spring, Sinai Peninsula, Egypt. *J. Acta Geophysica*, **59 (3)**, 633-656. DOI: 10.2478/s11600-011-0006-4

Abdel Zaher, M., Saibi, H., Nishijima, J., Fujimisty, Y., Mesbah, H., Ehara, S., (2012) Exploration and assessment of the geothermal resources in the Hammam Faraun hot spring, Sinai Peninsula, Egypt. *J. Asi. Earth. Sci*, **45**, 256–267.

Abdel Zaher, M., ElNuby, M., Ghamry, E, Mansour, K., Saadi, N.M., Atef, H., (2014) Geothermal studies in oilfield districts of Eastern Margin of the Gulf of Suez, Egypt. *NRIAG Journal*, **3**, 62-69.

Abuzied, S.M., Kaiser, M.F., Shendi, E.A.H. and Abdel-Fattah, M.I., (2020) Multi-criteria decision support for geothermal resources exploration based on remote sensing, GIS and geophysical techniques along the Gulf of Suez coastal area, Egypt. *J. Geothermics*, **88**, p.101893.

Ahmed, M, Sauck, W, Sultan, M, Yan, E, Soliman, F, Rashed, M., (2014) Geophysical constraints on the Hydrogeologic and structural settings of the Gulf of Suez rift-related basins: case study from the El Qaa Plain, Sinai, Egypt. *J. Surv Geophys*, **35**, 415–430. doi:10.1007/s10712-013-9259-6.

Araffa, S.A.S., Alrefaee, H.A, Nagy, M., (2020) Potential of groundwater occurrence using geoelectrical and magnetic data: A case study from south Wadi Hagul area, the northern part of the Eastern Desert, Egypt. *J. Afr. Earth. Sci*, **172**, 103970.

Atef, H., Abd El-Gawad, A. M., Abdel Zaher, M., Farag, K.S., (2016) The contribution of gravity method in geothermal exploration of southern part of the Gulf of Suez–Sinai region, Egypt. *NRIAG Journal*, **5**, 173–185.

Atya, M., Khachay, O., Abdel Latif, A., Khachay, O. y., El-Qady, G., and Taha, A., (2010) Geophysical contribution to evaluate the hydrothermal potentiality in egypt: case study: Hammam Faraun and Abu Swiera, Sinai, Egypt, *Earth. Sci. Res. J.*, **14 (1)**, 44-62.

Azab, A.A., El-Khadargy, A.A., (2013) 2.5-D gravity/magnetic model studies in Sahl el-Qaà area: Southwestern Sinai, Egypt. *J. Pur Ap.p Geophy.s*, **170**, 2207–2229. doi:10.1007/s00024-013-0650-5.

Blakely, R., (1995) Potential theory in gravity and magnetic applications. Cambridge University Press, Cambridge.

Bosworth, W., Huchon, P., McClay, K., (2005) The Red Sea and Gulf of Aden Basins. *J. Afr. Earth. Sci*, **43**, 334–378.

Bosworth, W., Khalil, S., Clare, A., Comisky, J., Abdela, H., Reed, T., Kokkoros, G., (2012) Integration of outcrop and subsurface data during the development of a naturally fractured Eocene carbonate reservoir at the East Ras Budran concession, Gulf of Suez, Egypt. *In:* Spence, G.H., Redfern, J., Aguilera, R., Bevan, T. G., Cosgrove, J. W., Couples, G.D., Daniel, J.M., (Eds) Advances in the Study of Fractured Reservoirs. Geological Society, London, Special Publications, 374p.

Boulos, F., (1990) Some aspects of the geophysical regime of Egypt in relation to heat flow, groundwater and microearthquakes. In: Said, R. (Ed.), The Geology of Egypt, A. A. Balkema/Rotterdam/Brookfield, pp. 61-89.

Chowdhary, L.R., Taha, S., (1987) Geology and Habitat of Oil in Ras Budran Field, Gulf of Suez, Egypt. *AAPG Bulletin.*, **71**, 1274-1293.

Cooper, G.R.J., Cowan, D.R., (2006) Enhancing potential field data using filters based on the local phase. *J. Comput. Geosci.*, **32**, 1585–1591.

El-Fiky, A.A., (2009) Hydrogeochemistry and Geothermometry of Thermal Groundwater from the Gulf of Suez Region, Egypt. *J. King Abdulaziz Univ.*, **20**, 71-96.doi: 10.4197/Ear.20-2.5

El-Hateel, S.M. (2013). Subsalt imaging and structure interpretation using 3D Pre-stack Depth Migration in the Gulf of Suez, Ras Budran Field: AAPG/SEG Exploration of Subsalt Structures in Rift Basins Workshop, Dead Sea, Jordan.

El-Qady, G., Ushijima, K., El-Sayed A., (2000) Delineation of a geothermal reservoir by 2D inversion of resistivity data at Hammam Faraun area, Sinai, Egypt. *Proc. Wor. Geoth. Cong.*, 1103-1108.

El-Qady, G., Salem, A., Aboud, E., Khalil, A., Ushijima, K., (2005) Geothermal Reconnaissance Study for Sinai Peninsula, Egypt. *Proc. Wor. Geoth. Cong.*, 1-7.

Garfunkel, Z., Bartov, Y., (1977) The tectonics of the Suez rift. *Geol. Surv. of Israel*, **71**, 1–44.

Goldstein, B.A., Hiriart, G., Tester, J., Bertani, B., Bromley, R., Gutierrez-Negrin, L. C.J., Huenges, E.H., Ragnarsson, A., Mongillo, M.A., Muraoka, M.A., Zui, V.I., (2011) Great expectations for geothermal energy to 2100. Proceedings, 36th Workshop on Geothermal Reservoir Engineering, Stanford University, Stanford, California, January 31 - February 2, 2011, SGP-TR-191, 8 p.

Harding, T.P., (1984) Graben hydrocarbon occurrences and structural styles. *AAPG Bulletin.*, **68**, 333–362.

Horner, R.D., (1951) Pressure build-up in wells. *Proc. of 3rd Wor. Petr. Cong., The Hague, the Netherlands*, **34**, 316.

Issar, A., Rosenthal, E., Eckstein, Y., Bogoch, R., (1971) Formation waters, hot springs and mineralization phenomena along the eastern shore of the Gulf of Suez. *Bull. of the Int. Ass. of Sci. Hydr,* **16**, 25–44.

Jackson, C., Gawthrope, R., Young, M., Stewart, J., Pivnik, D., Sharp, L., (2002) Rift compartmentalization and evolution of tilted fault blocks as expressed by the lower Miocene of Abu Zeneima and Nukhul formations, Suez Egypt. *Int. Pet. Conf. and Exh.*, Cairo, Egypt.

Lashin, A., (2013) A preliminary study on the potential of the geothermal resources around the Gulf of Suez, Egypt. *Arab. J. Geosci.,* **6**, 2807–2828.doi: 10.1007/s12517-012-0543-4.

Morgan, P., Boulos, K., Swenberg, C.A., (1983) Regional geothermal exploration in Egypt. *J. Geophys. Pros*, **31**, 361-376.doi: 10.1111/j.1365-2478.1983.tb01059.x

Moustafa, A.R., Abdeen, M., (1992) Structural setting of the Hammam Faraun Block, eastern side of the Suez rift. *J. Univ. of Kuwait Sci,* **19**, 291–310.

Peters, K.E., Nelson, P.H., (2009) Criteria to Determine Borehole Formation Temperatures for Calibration of Basin and Petroleum System Models, Adapted from poster presentation at *Ame. Ass. of Pet. Geol. Annual Convention and Exhibition, Denver, Colorado, USA*, 27p.

Pivnik, D.A., Ramzy, M., Steer, B.L., Thorseth, J., El Sisi, Z., Gaafar, I., Garing, J.D., Tucker, R.S., (2003) Episodic growth of normal faults as recorded by syn-tectonic sediments, July oil field, Suez rift, Egypt. *AAPG Bulletin.*, **87**, 1015–1030. doi: 10.1306/02050301100

Said, R., (1962) The geology of Egypt: Amsterdam, Elsevier, 377 p.

Spector, A., Grant, F.S., (1970) Statistical models for interpreting aeromagnetic data. *J. Geophys*, **35**, 293–302.

Tanaka, A., Okubo, Y., Matsubayashi, O., (1999) Curie point depth based on spectrum analysis of the magnetic anomaly data in East and Southeast Asia. *J. Tectonophys*, **306**, 461–470.

Tewfik, N., Harwood, C., Deighton, I., (1992) The Miocene, Rudeis and Kareem formations of the Gulf of Suez. *Aspects of Sedimentology and Geohistory*,11th Petroleum Exploration and Production Conference, Cairo, **1**, 84–113.

Tester, J.W., Anderson, B.J., Batchelor, A.S., Blackwell, D.D., Dipippo, R., Drake, E.M., Garnish, J., Livesay, B., Moore, M.C., Nichols, k., Petty, S. Toksoz, M.N., Veatch, R.W., Baria, R., Augustine, C. Murphy, E., Negraru, P., Richards, M., (2007) Impact of enhanced geothermal systems on US energy supply in the twenty-first century. *Philosophical Transactions of the Royal Society,* **365**, 1057-1094. doi: 10.1098/rsta.2006.1964

Thompson, T. L., (1976) Plate tectonics in oil and gas exploration of continental margins. *AAPG Bulletin*, **60**, 1463-1501.doi: 10.1306/C1EA3884-16C9-11D7-8645000102C1865D

United States Geological Survey, (1998) The Red Sea Basin Province, *Open File Report*, **99**-50A.

Waples, D.W., Pacheco, J., Vera, A., (2004) A method for correcting log-derived temperatures in deep wells, calibrated in the Gulf of Mexico. *J. Petr. Geosci.*, **10**, 239–245. doi: 10.1144/1354-079302-542

Wijns, C., Perez, C., Kowalczyk, P., (2005) Theta map: Edge detection in magnetic data: *J. of Geophys*, **70**. L39-L43.

Zahra, H.S., Nakhla, A.M., (2015) Deducing the subsurface geological conditions and structural framework of the NE Gulf of Suez area, using 2-D and 3-D seismic data. *NRIAG Journal,* **4**, 64–85. doi.org/10.1016 /j. nrjag.2015.04.003

الضوابط التركيبية والطباقية على النظام الحراري الأرضي لخليج السويس، مصر، كما تم الكشف عنها بالبيانات الجيوفيزيائية ودرجة حرارة قاع البئر

حامد عبدالحميد حامد الرفاعي
قسم الجيولوجيا، كلية العلوم، جامعة كفر الشيخ، مصر

تم تحليل قياسات درجة حرارة قاع البئر في منطقة خليج السويس بمصر ، لتقييم معاملات الطاقة الحرارية الأرضية لمنطقة الدراسة. يتراوح التدرج الحراري من ٢٢ إلى 44 درجة مئوية / كم ، وتتدفق الحرارة من ٤٥ إلى ١١٨ ميغاواط / م ٢. يتوافق أعلى تدرج وتدفق حراري مع سواحل خليج السويس. يظهر التدرج الحراري العالي والتدفق الحراري العالي في منطقة حمام فرعون - رأس بدران وجنوب أبو زنيمة على الساحل الشرقي للخليج. كما يظهر التدرج الحراري العالي والتدفق الحراري العالي في منطقة رأس غارب على الساحل الغربي للخليج. التدرجات الحرارية المنخفضة والتدفق الحراري المنخفضة يتوافقان مع حوض خليج السويس. تم تفسير القطاعات السيزمية للكشف عن تأثير الوضع التركيبي المحلي والتتابع الطباقي على معاملات الطاقة الحرارية الأرضية. تم تحليل خريطة شذوذ البوجير لتحديد الوضع التكتوني الإقليمي وتأثيره على نظام الطاقة الحرارية الأرضية في خليج السويس. تم استخدام البيانات المغناطيسية لحساب نقطة عمق كوري وفحص أي علاقة أو ارتباط مع المعلمات الحرارية الأرضية للمنطقة. توجد الخزانات الحرارية الجوفية في جنوب أبو زنيمة، وحمام فرعون، ورأس غارب على ساحلي خليج السويس. من الممكن حفر آبار حرارية للحصول على المياه الحرارية ، والتي لها استخدامات متنوعة.